RIEMANNIAN GEOMETRIES OF VISUAL SPACE: VARIABLE CURVATURE AND HORIZON

Jacek Turski*
Department of Mathematics and Statistics
University of Houston-Downtown
Houston, TX 77002
turskij@gmail.com

June 2, 2022

ABSTRACT

Two dimensional (2D) images of light beams reflected off the objects in space impinge on the retinal photoreceptors of our two laterally separated eyes. Nevertheless, we experience our visual percept as a single 3D entity—our visual world that we tend to identify with physical world. However, experiments point to different geometries in these two worlds. Using the binocular system with the asymmetric eyes (AEs), this article studies the global geometric aspects of visual space in the Riemannian geometry framework. The constant-depth curves in the horizontal field of binocular fixations consist of families of arcs of ellipses or hyperbolas depending on the AE parameters and the eyes' fixation point. For a single set of AE's parameters, there is a unique symmetric fixation at the abathic distance such that the constant-depth conics are straight frontal lines. Critically, the distribution of the constant-depth lines is independent of such fixations. In these cases, a two-parameter family of the Riemann metrics is proposed based on the retinal topography and simulated constant-depth lines. The obtained geodesics for a subset of metric parameters include the incomplete geodesics that give finite distances to the horizon. The Gaussian curvature of the phenomenal horizontal field is analyzed for all the metric parameters. The sign of the curvature can be inferred from the global behavior of the constant-depth ellipses and hyperbolas only when for the metric parameters for which the constant-depth frontal lines at the abathic distance fixations are geodesics.

***K*eywords** Binocular correspondence, asymmetric model eye, iso-disparity conics, visual space, Riemannian geometry, metric tensor, incomplete geodesics, Ermakov-Pinney differential equations, curvature

1 Introduction

Our two laterally separated eyes' retinal photoreceptors receive slightly different 2D projections of photons reflected off objects located in physical space. The brain's immense number of neurons process these proximal stimuli to enhance our spatial vision with depth, shape, and sensation of being immersed in the 3D environment. How is this feat achieved? To this end, two unique small retinal areas, each in a different eye, share a common subjective visual direction when separately stimulated. These retinal areas are called corresponding retinal elements determined by the nonius paradigm. We consider each pair of the binocular correspondence as having zero disparity. For a given binocular fixation, the horopter is the locus of points in space such that each point on the horopter projects to a pair of corresponding retinal elements. Thus, it is the distal stimuli curve of zero-disparity.

Further, a small object located away from the horopter has nonzero disparity and, in general, is perceived as two objects. However, the brain fuses its disparate images into a single percept for an object close to the horopter. Then the extracted disparity is used by the brain to create our sense of depth relative to the horopter. Even the objects located farther from the horopter, which leads to double vision, convey the sense of depth [41].

*Professor Emeritus

More essentially, the brain uses the difference in the horizontal disparity between two spatial points to sense the relative depth and, hence, our perception of objects' shapes and their locations in 3D space [61], that is, stereopsis and visual space geometry. Thus, stereopsis is supported mainly by the horizontal retinal correspondence and, hence, the longitudinal horopter because of the lateral separation of eyes. The outcome of the above outlined physiological processes is the beholder's three-dimensional visual experience combined with other perceptual modalities and transcended by higher cognitive processing.

Although the study of visual space has had a long history, see [20] for a review, the geometric relationship between visual space and stimuli-containing physical space remains unresolved. The main reason is that the spatial relations in phenomenal space, such as depth and size, are, in general, task-dependent and influenced by contextual factors, our memory, learning, and even expectations. However, the binocular disparity, which is one of many potential cues to depth used by the brain, provides the most compelling depth cue sufficient for stereopsis with no explicit recognition of a scene's geometric forms [28]. This perception based on binocular disparity alone, referred to as the Cyclopean perception, is unaffected by other factors.

This article concerns our phenomenal geometry based on the binocular disparity before the involvement of psychological processes. To this end, with the help of the geometric theory of the binocular system with the asymmetric eye (AE) model developed in [53, 54], I investigate here the global aspects of spatial perception based on the relative disparity in the framework of Riemannian geometry. The appendix introduces the most basic concepts of Riemannian geometry in one global chart that is imposed in this study by a stationary, upright head. For the alternative line of research in visual perception, namely psychophysics, please refer to a review in [45].

The horopteric conics constructed and simulated in [54], that reliably model the empirical horopters with their geometry fully integrated with eyes movement, are extended here to the families of iso-disparity conics. These families provide numerical values of relative disparity (and hence stereopsis) for a stationary, upright head with the eyes converging on the points of the horizontal binocular field of fixations.

For almost all bifoveal fixations on points of the horizontal binocular field, the iso-disparity curves consist of either a family of hyperbolas or ellipses, depending on both the AE' two parameters: the fovea displacement from the posterior pole and the crystalline lens tilt relative to the cornea, and the location of the point of fixation. For every pair of parameters of the AE, a unique symmetric fixation furnishes the family of iso-disparity frontal straight lines. This fixation is said to be at the abathic distance and is called the resting eyes posture. The critical fact used in modeling the phenomenal Riemann metric is that the distribution of iso-disparity lines does not depend on the abathic distance.

However, to model perceived relative depth from the iso-disparity conics, their analysis should be combined with the fundamental aspects of the architecture of the human visual system. Still, there is no theory based on first principles reflecting this architecture that can describe how relative depth varies with disparity and distance. Consequently, the analysis of the simulated iso-disparity frontal lines and the retinal photoreceptors' topography led us to two postulates: (1) a one-parameter model of the perceived relative depth and (2) a one-parameter model of the relative width. These two postulates define a two-parameter family of Riemann metric tensors in the horizontal plane of binocular fixations.

In the Riemannian geometry framework, the direct solutions of the geodesics differential equations are obtained for a subset of the metric tensor parameters when the iso-disparity lines are geodesics. Further, the two-parameter family of metric tensors is transformed into the one-parameter family of conformally equivalent metric tensors. Then, the geodesics' differential equations become the Ermakov-Pinney equations and are solved explicitly. In all cases mentioned above, the curvature is zero and, therefore, a two-dimensional visual space is flat. However, almost all geodesics are incomplete in the Cyclopean gaze direction, each giving a finite distance to the horizon. Finally, the solution of geodesic differential equations is obtained for one case of parameters that gives the negative Gaussian curvature of the hyperbolic half-plane model. However, in this case, the horizon is infinitely away.

The consequences of the results obtained in the Riemannian geometry framework on modeling global aspects of spatial perception based on simulated iso-disparity conics are discussed in the last section. The iso-disparity conics are obtained by extending the geometric theory of the horopters resembling the empirical horopters developed in [54]. This reference, together with [52] finally resolved the horopter controversy that has been prevalent ever since the modern history of the horopter started by Aguilonius in his Six Books of Optics published in 1613. This controversy is discussed in Appendix B.

2 Resting Eyes Posture and Retinal Correspondence

Binocular vision space is organized through corresponding points. The correspondence of retinal elements as described in the first section, forms the basis of the nonius paradigm for a direct determination of the corresponding retinal elements [40, 48]. All other methods, as reviewed in [56, 57], are indirect and less reliable.

The retinal correspondence cannot be readily measured [57] as well as it cannot be directly obtained from geometrical models. The main reason is the beholder eye's asymmetry: the corresponding points are compressed in the temporal retinae relative to those in the nasal retinae [23, 49].

This situation changed when the geometric theory of the binocular system with the asymmetric eyes (AEs) was developed in [53, 54], which advanced Ogle's classic theory of 1932 [39]. Ogle's theory introduced the horopters in an ad-hock way as conic sections with free parameters. They were also incorrectly passing through the eyes' rotation centers rather than the nodal points. In contrast, the horopteric conics in [54] are rigorously constructed in the binocular system with the AEs and correctly pass through the nodal points. Crucially, their geometry is integrated with the eyes' movement in the binocular field of horizontal fixations.

The AE model is comprised of the fovea's displacement from the posterior pole by angle $\alpha = 5.2^\circ$ and the crystalline lens' tilt by angle β. Angle α is relatively stable in the human population and angle β varies between -0.4° and 4.7°, cf. the discussion in [53]. The angles α and β are depicted in Figure 1. In the human eye, the fovea's displacement from the posterior pole (located at the point where the optical axis intersects the retina in Figure 1) and the cornea's asphericity contribute to optical aberrations that the lens' tilt then partially compensates for [2].

The geometric theory of the binocular system with AEs fully specifies the retinal correspondence asymmetry in terms of AE's parameters and the point of fixation. It was demonstrated in simulations of horopteric conics [54] starting from the resting eyes posture shown in Figure 1.

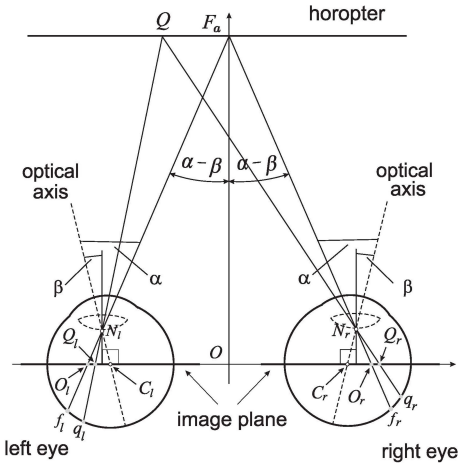

Figure 1: The linear horopter passing through the fixation F_a at the abathic distance $d_a = |OF_a|$. In this eyes' posture, the image planes, which are parallel to the lenses' equatorial planes, are coplanar. The point F_a projects through the nodal points N_r and N_l to the foveae f_r and f_l while the point Q on the horopter projects to the retinal corresponding points q_r and q_l and to points Q_r and Q_l in the image plane. The subtense σ_a at F_a is given by $2(\alpha - \beta)$ [54].

The resting eyes posture, or just the resting eyes, refers to the AEs fixating at the abathic distance. The image plane in the AE model is parallel to the lens's equatorial plane and is passing through the eye's rotation center. Figure 1 shows the eyes' posture in which the image planes are coplanar, and the horopter is a straight frontal line passing through the fixation point at the abathic distance. This distance numerically corresponds to the eyes' resting vergence posture [27], which explains the name used. Notably, because the eye muscles' natural tonus resting position serves as a zero-reference level for convergence effort, [14], this posture is identified in [54] with the eyes' binocular primary position used in oculomotor research without its precise definition.

I recall that the distribution of the retinal corresponding points q_r, q_l is asymmetrical with respect to the foveae f_r and and f_l such that $|q_r f_r| \neq |q_l f_l|$, see Figure 1. It is demonstrated in [54], that the distribution of these corresponding points projected into the image planes of each AE, Q_r, Q_l, satisfy $|Q_r O_r| = |Q_l O_l|$ where O_r and O_l are projected foveae f_r and f_l, respectively. It is proved in [54] that this symmetry on the image plane is preserved for all other fixations. Thus, unknown (asymmetric) retinal correspondence can be entirely formulated on the image plane of the AE in terms of the asymmetry parameters.

The abathic distance $d_a = |OF_a|$ to the fixation point F_a in the eyes' resting vergence posture was obtained in [54] as follows:

$$d_a = \frac{a\cos(\alpha-\beta)+0.6\sin\alpha}{\sin(\alpha-\beta)}, \tag{1}$$

where $2a = 6.5$ cm is the ocular separation and 0.6 cm is the distance of the nodal point from the eyeball's rotation center.

3 Simulation of Iso-Disparity Curves

For an observer with a stationary, upright head and binocular fixations in the horizontal plane, the coordinate system consists of the y-axis passing through the eyes' rotation centers and the head z-axis formed by the intersection of the midsagittal plane with the horizontal visual plane. The x-axis points up for the right-handed coordinate system, which determines the angle's sign in Figure 4.

The iso-disparity points are first specified on the image planes of the AEs when the eyes are in the resting posture shown in Figure 1. Referring to this figure, points Q_r and Q_l that are on the same side of the respective centers O_r and O_l and of the same distance are covering the non-uniformly distributed corresponding retinal elements q_r and q_l. The corresponding points back-projected through the nodal points to physical space give the point Q on the horopter line.

The iso-disparity lines in physical space are constructed in the eyes' resting posture as follows. The points $Q_r + \delta_0$ and Q_l on the y-coordinate line, when back-projected, gives the crossed point on the δ_0-disparity line. Similarly, the points $Q_r - \delta_0$ and Q_l, when back-projected, give the uncrossed point on the $-\delta_0$-disparity line. The simulations of the iso-disparity conics of a constant relative disparity are carried out in *GeoGebra*. Please, refer to [54] for the details of the geometric constructions of the hyperbolic conics shown in this section figures.

The iso-disparity lines for the eyes fixating at the two different values of the abathic distance d_a are shown in Figure 2: (a) $d_a = 40.2$ cm and (b) $d_a = 99.61$ cm. The horopters are shown in red lines. This figure demonstrates invariance of the iso-disparity distribution for the given relative disparity $\delta_0 = 0.00355$ cm: the spacing is a function of the relative disparity and the egocentric distance but is independent of the AE's parameters that define the eyes' resting posture at the abathic distance d_a.

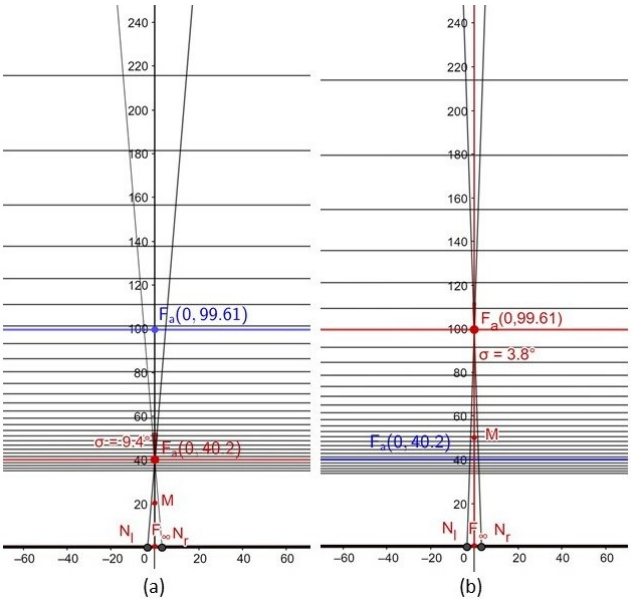

Figure 2: The iso-disparity lines for the eyes' resting posture with the abathic distance given in (1) for the respective AE lens tilt β: (a) the abathic distance is $d_a = 40.2$ cm for $\beta = 0.5°$. (b) the abathic distance is $d_a = 99.61$ cm for $\beta = 3.3°$. Shown in blue are the lines in the opposite eye fixation matching the horopter red lines. This demonstrate the invariance of the iso-disparity lines' distribution. The subtense angles at F_a (shown in red color) are $\sigma = 2(\alpha - \beta)$ for the corresponding values of β and $\alpha = 5.2°$.

Figure 3 and Figure 4 show how the iso-disparity lines for the two binocular systems, one with the abathic distances of $d_a = 40.2$ cm and the other with the abathic distance of $d_a = 157.75$ cm, are transformed when each fixation changes

to fixations at the same distance of $d_a = 99.61$ cm. Figure 3 shows the iso-disparity hyperbolas in panel (a) and the iso-disparity ellipses in panel (c) for the new symmetric fixations. They are compared in panel (b) to the iso-disparity lines for fixation at the abathic distance $d_a = 99.61$ cm. Their asymmetrical fixations of the same distance along the Cyclopean rays are shown in Figure 4. The direction of the Cyclopean ray specifies the orientation of the horopteric conics [54] and, therefore, the orientations of the iso-disparity conics for a given fixation.

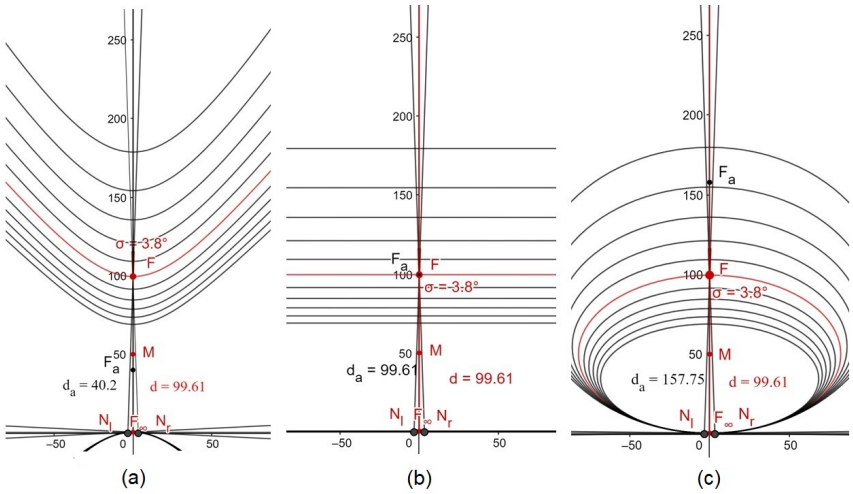

Figure 3: The iso-disparity conics for the three binocular systems with AEs fixating symmetrically at $d = 99.61$ cm: (a) the system with the abathic distances of $d_a = 40.2$ cm. (b) the system with the abathic distance $d_a = 99.61$ cm. (c) the system with the abathic distances of $d_a = 157.75$ cm.

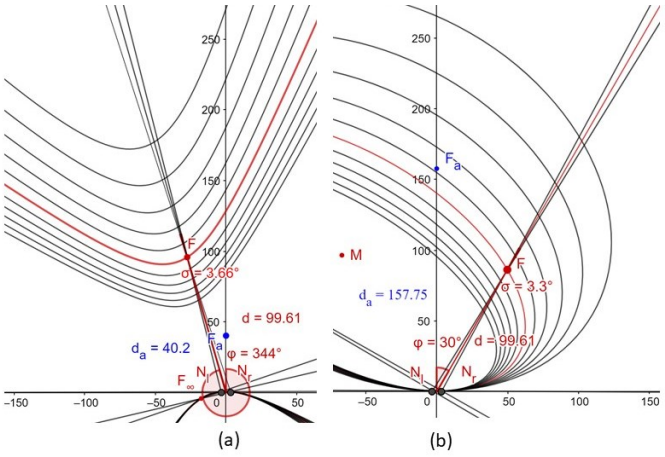

Figure 4: The iso-disparity conics for two asymmetric fixations: (a) Iso-disparity hyperbolas when the AEs with the abathic distance $d_a = 40.2$ cm fixate at $16°$ of azimuthal angle and 99.61 cm away along the Cyclopean direction. (b) Iso-disparity ellipses when the AEs of the abathic distance $d_a = 157.75$ cm fixate at $-30°$ of azimuthal angle and 99.61 cm away along the Cyclopean direction. The Cyclopean direction very well approximates the conic orientation [54].

4 Numerical Analysis of Iso-disparity lines for Resting Eyes

From the simulations shown in Figure 2 for the disparity step of $\delta_0 = 0.00355$ cm, I calculate the distance Δz_i and midpoint z_i between the consecutive iso-disparity lines to approximate how the depth of iso-disparity lines changes with the distance from the head in the gaze's direction. The points $(z_i, \Delta z_i)$ for different abathic distance eyes fixations lie on the graph of a single quadratic function

$$\Delta z(z, \delta_0) = 0.000892 z^2 \tag{2}$$

shown in Figure 5.

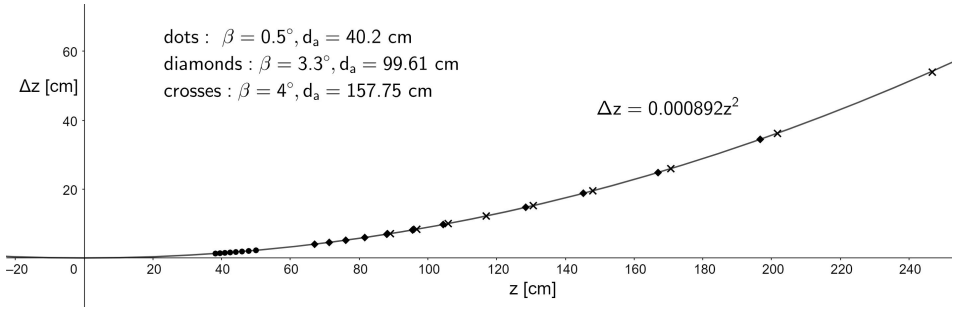

Figure 5: For the simulations shown in Figure 3, the points $(z, \Delta z)$ are plotted for three different abathic distance fixations: $d_a = 40.2$ cm (dots), $d_a = 99.61$ cm (diamonds), and $d_a = 157.75$ cm (crosses).

The data presented in Figure 5 specify more precisely the iso-disparity invariance of the abathic distance of the resting eyes.

To investigate how the iso-disparity lines distribution depends on the disparity value, I compare simulated iso-disparity lines for disparity difference $\delta_0 = 0.00355$ cm with lines simulated for disparity $\delta = (1/5)\delta_0 = 0.00071$ cm, each for the abathic distance $d_a = 99.61$ cm. The result of these two simulations is shown in Figure 6.

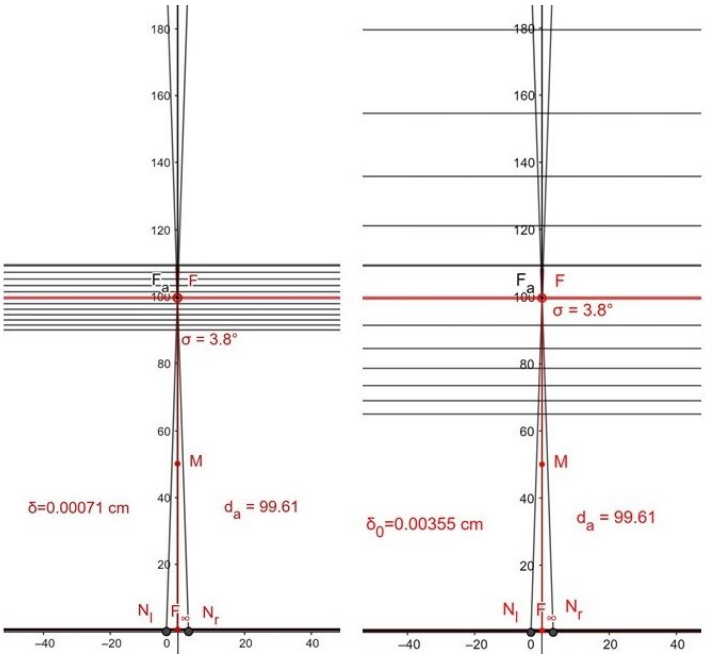

Figure 6: The is-disparity lines for $d_a = 99.61$ cm with different disparity values; on the right, $\delta_0 = 0.00355$ cm, while on the left, $\delta = 0.00071$ cm.

We can see that each space between the neighboring iso-disparity lines for disparity $\delta_0 = 0.00355$, shown on the right in Figure 6, is filled by an additional five iso-disparity lines for disparity $\delta = 0.00071$, shown on the left in Figure 6. Thus, the relation

$$\Delta z(z, \delta) = 0.000178z^2 = \frac{1}{5}0.000892z^2, \tag{3}$$

can be predicted from the simulations and verified numerically. In fact, substituting $d_a = 99.61$ cm for z in (3), we obtain,

$$\begin{aligned}\Delta z(d_a,\delta) &= 0.000178 d_a^2 = 1.77 \text{ cm} \\ &= \frac{1}{5}0.000892 d_a^2 = \frac{1}{5}8,85 \text{ cm},\end{aligned}$$

which agree with the simulations shown in Figure 6.

The above discussion of simulations demonstrate that for any $z > 0$, disparity δ, and $h > 0$,

$$\Delta z(z, h\delta) = h\Delta z(z, \delta),$$

and this relation can be scaled down to the value of the disparity imposed by the foveal distribution of photoreceptors.

I conclude that the interval between iso-disparity lines for the disparity difference $\delta = h\delta_0$ satisfies the relation,

$$\frac{\Delta z(z, h\delta_0)}{z^2} = h0.000892 = h\frac{8.85}{(99.61)^2}$$

where 8.85 cm is the distance between the horopter line and the $-\delta_0$-disparity line when $d_a = 99.61$ cm for $\beta = 3.3°$.

I choose the h value such that $\Delta z(d_a, h\delta_0)$ gives the depth resolution at the fovea where the cone-to-cone spacing is about 2.7×10^{-4} cm, which gives the corresponding spacing of 10^{-4} cm on the image plane of the AE. Given that $\delta_0 = 0.00355$ cm, we obtain $h = 10^{-4}/3.55 \times 10^{-3} \approx 1/35$. Thus, for $h = 1/35$,

$$\Delta z(d_a, h\delta_0) = h0.000892 d_a^2 = 2.5 \times 10^{-5} d_a^2. \tag{4}$$

To simplify notation, I denote $\Delta z(z, (1/35)\delta_0)$ by $\Delta z(z)$. Then, we obtain from (4): $\Delta z(d_a) \approx 0.25$ cm for $d_a = 99.61$ and $\Delta z(d_a) \approx 0.04$ cm for $d_a = 40.2$.

Remarkably, under ideal conditions, the best observers' disparity thresholds are as low as 3 seconds of arc, representing the detection of 0.01 mm at 25 cm [60], which is about one order lower than predicted by (4). It is an example of hyperacuity when the acuity threshold is smaller than the diameter of the photoreceptor (cone) in the foveal center, which should imply the best foveal resolution close to 1 minute of arc [11].

5 Metric Tensor for Resting Eyes: Inner Product, Angle and Length

The reader should recall that the coordinate system (y, z) in the field of binocular fixations B consists of the y-axis passing through the eyes' rotation centers and the head z-axis formed by the intersection of the midsagittal plane with the horizontal plane passing through the fixation point and the eyes' nodal points and rotation centers. The point $(0, \xi)$ is the closest point on which the eyes can converge due to obstruction by the protruded nose. Further, the fixations are neurally restricted to the azimuthal range $\pm 45°$ [18]. Thus, the set B is the convex region bounded by two rays with the intersection point $(0, \xi)$ and each inclined by $45°$ with the z-axis.

For a fixation point, the chart for the binocular plane is the whole set B. For every fixation $(y, z) \in B$, I want to find the corresponding scalar product on the tangent plane, R^2, with its origin at (y, z), using the biologically motivated geometric theory of human binocular perception developed in [54]. These families of scalar products will define the Riemannian geometries of visual space, each dependent on the AEs parameters and the point of binocular fixation. Appendix A outlines the underlying notions of Riemannian geometry.

In order to model perceived relative depth, the simulations must be combined with the fundamental features of the human visual system's architecture, which include the cones' eccentricity dependent density and the convergence of the photoreceptors on the ganglion cells, which is 1-to-1 in the central fovea and which approaches 200-to-1 in the periphery. Related to this issue, the concept of receptive fields becomes essential. Visual information is sent from the eyes along the ganglion cells' axons and arrives, mainly, at the primary visual cortex, where it is retinotopically mapped with a significant magnification of the foveal region and scaled logarithmically with retinal eccentricity [37].

Moreover, human disparity contains two components: fine disparity and coarse disparity [38]. Fine disparity allows us to determine the depth of objects in the central visual area where disparate images are fused into a single percept (Panum's fusional area). Coarse disparity provides stereopsis from disparities well beyond the fusible range. It is still useful for depth perception for moderately large disparities, even for double images but is only clearly signed with a vague impression of depth magnitude for very large disparity values [6, 62]. Importantly, coarse disparity creates our sense of being immersed in the ambient environment [4].

No theory based on first principles is available to describe how perceived relative depth varies with disparity and distance. Therefore, using the above numerical analysis of simulated iso-disparity lines and the above discussion, I postulate that the relative depth element δd in visual field of fixations approximately satisfies the relation

$$\delta d(z) = \rho\left(\frac{d_a^2}{z^2}\Delta z(z)\right) = \frac{d_a^{2-\eta}}{z^{2-\eta}}\delta z \tag{5}$$

where $0 \leq \eta \leq 1$ and $\delta z = \Delta z(d_a)$. It is assumed that the functional ρ accounts for the anatomical and physiological aspects of the human visual system.

Further, similarly, I assume the line element $\delta\lambda$ along the iso-disparity line as follows

$$\delta\lambda(z) = \frac{d_a^{1-\mu}}{z^{1-\mu}}\delta y. \tag{6}$$

where $0 \leq \mu \leq 1$.

Finally, combining it with (5), I obtain the line element.

$$\delta s^2 = \frac{d_a^{2-2\mu}}{z^{2-2\mu}}\delta y^2 + \frac{d_a^{4-2\eta}}{z^{4-2\eta}}\delta z^2. \tag{7}$$

.

The set B has the Cyclopean visual metric determined by a map

$$g : (y, z) \in B \longrightarrow g_{(y,z)} \in M_2, \tag{8}$$

where $g_{(y,z)}$ is the Riemann metric tensor obtained from the line element (7),

$$g_{(y,z)} = \begin{pmatrix} \frac{d_a^{2-2\mu}}{z^{2-2\mu}} & 0 \\ 0 & \frac{d_a^{4-2\eta}}{z^{4-2\eta}} \end{pmatrix};\ \ 0 \leq \mu \leq 1,\ 0 \leq \eta \leq 1, \tag{9}$$

and M_2 is the set of all real symmetric positive defined 2×2 matrices.

This study emphasizes modeling the phenomenal geometry's global aspects that can be studied in the Riemannian geometry framework and tested in experiments. Some of the global aspects of this phenomenal geometry seem to agree with the experimental results reported in the literature and are discussed in Section 10.

The visual metric tensor defines an inner product on each tangent plane $T_{(y,z)}B$, the tangent plane R^2 at (y, z) that has the origin at this point. Because $(0, 0) \notin B$, the map g in (8) is a smooth function on B. The inner product is usually written $\langle\partial_j, \partial_k\rangle = g_p(\partial_j, \partial_k) = g_{jk}(p)$ where $p = (y, z)$ and each index runs over y and z for the vector basis $\partial_y, \partial_z \in T_{(y,z)}B$. Thus, the length of the vector $V = \left(v^i\right)$ is $||V|| = \sqrt{\langle V, V\rangle} = \sqrt{\sum_{i,j} g_{ij}v^i v^j}$ and the angle between vectors U and V can be obtained from $\cos\theta = \langle U, V\rangle/||U||||V||$.

Although I use standard Riemannian geometry notation for writing the basis vectors, it should be understood that for the coordinates (y, z), $\partial_y = (1, 0)$, and $\partial_z = (0, 1)$.

The pair (B, g) is a global chart on the binocular field that allows computing the length of vectors in tangent spaces and, therefore, the length of curves in B.

The perceived direction of the point does not depend on whether the stimulus reaches the retinal element in one eye or its corresponding element in the other eye alone or whether it reaches both the corresponding element simultaneously [57]. For a fixation point in B, the monocular perception from outside of B is still available. However, stereopsis is not available in the region outside of B.

6 Geodesic Differential Equations for Resting Eyes

For an excellent exposition of the Riemannian geometry framework, please refer to [13]. I start by writing the defining expressions for the Christoffel symbols,

$$\Gamma^i_{jk} = \sum_l \frac{1}{2}g^{il}(g_{lk,j} + g_{jl,k} - g_{jk,l}), \tag{10}$$

where $(g^{il}) = (g_{il})^{-1}$ is the inverse matrix.

Then, a geodesic is a curve $\gamma(t) = (x^i(t))$ whose the covariant derivative of the velocity vector is zero, see Appendix A.3,

$$\frac{\nabla(dx^i(t)/dt)}{dt} = \frac{d^2x^i}{dt^2} + \sum_j \sum_k \Gamma^i_{jk} \frac{dx^j}{dt}\frac{dx^k}{dt} = 0. \tag{11}$$

In the notation used here, the tensor matrix (9) entries are

$$g_{yy} = d_a^{2-2\mu}/z^{2-2\mu} \quad \text{and} \quad g_{zz} = d_a^{4-2\eta}/z^{4-2\eta}. \tag{12}$$

Adapting this notation used for coordinates (y, z), non-zero expressions (10) are the following:

$$\Gamma^y_{yz} = \Gamma^y_{zy} = \frac{g_{yy,z}}{2g_{yy}} = -\frac{1-\mu}{z}, \tag{13}$$

$$\Gamma^z_{yy} = -\frac{g_{yy,z}}{2g_{zz}} = (1-\mu)\frac{z^{1+2\mu-2\eta}}{d_a^{2+2\mu-2\eta}}, \tag{14}$$

and

$$\Gamma^z_{zz} = \frac{g_{zz,z}}{2g_{zz}} = -\frac{2-\eta}{z}. \tag{15}$$

For the notation used in this paper: $x^1 = y$ and $x^2 = z$, the geodesic differential equations (11) are the following

$$y'' - 2\frac{1-\mu}{z}y'z' = 0 \tag{16}$$

and

$$z'' + (1-\mu)\frac{z^{1+2\mu-2\eta}}{d_a^{2+2\mu-2\eta}}y'^2 - \frac{2-\eta}{z}z'^2 = 0, \tag{17}$$

where the 'prime' means '$\frac{d}{dt}$'.

The differential equations can be explicitly solved for $\mu = 1$. Because in this case, $y'' = 0$, the iso-disparity lines are geodesics. The solutions will be obtained in Section 7.1.

6.1 The Ermakov-Pinney Equations

The first equation (16) can be one time integrated, which then the initial conditions $z(0) = z_0$ and $y'(0) = k_1$ gives

$$y' = \frac{k_1}{z_0^{2-2\mu}} z^{2-2\mu} \tag{18}$$

After substituting (18), the second equation (17) can be written as

$$z'' + \frac{(1-\mu)k_1^2}{z_0^{4-4\mu} d_a^{2+2\mu-2\eta}} z^{5-2\mu-2\eta} - \frac{2-\eta}{z}z'^2 = 0. \tag{19}$$

These geodesic differential equations can be solved when $\mu = \eta$ by transforming (19) into the celebrated Ermakov-Pinney equation that has a general solution despite being a nonlinear differential equation, which is very special for nonlinear equations [17, 32, 42].

Theorem 1. *If $a = 1/(1-\eta)$, $\eta \neq 1$ and $\mu = \eta$, then the equation (19) under the change of variables $w(t) = z(t)^{-1/a}$ transforms into the Ermakov-Pinney equation $w'' - C^2 w^{-3} = 0$. All metrics with $\mu = \eta$ are conformally equivalent.*

Proof. Let $z = w^{-a}$, then by substituting $z' = -aw^{-a-1}w'$, $z'' = -aw^{-a-1}w'' + a(a+1)w^{-a-2}w'^2$ into (19) we obtain

$$w'' - (a+1)w^{-1}w'^2 + (2-\eta)aw^{-1}w'^2 - \frac{(1-\mu)k_1^2}{az_0^{4-4\mu}d_a^{2+2\mu-2\eta}}z^{-4a+2a\mu+2a\eta+1} = 0.$$

By assuming $a+1 = (2-\eta)a$, which gives $a = 1/(1-\eta)$, we eliminate the second and third terms. Next, by requiring that the exponent in the last term is -3, that is, $-4a + 2a\mu + 2a\eta + 1 = -3$. This last expression simplifies to $\mu = \eta$ after $a = 1/(1-\eta)$ is used. Thus, we arrive at w''

$$w'' - C^2w^{-3} = 0 \tag{20}$$

and

$$C^2 = \frac{(1-\eta)^2k_1^2}{d_a^2z_0^{4-4\eta}}.$$

The conformal equivalence of metrics follows from the observation that for $\mu = \eta$,

$$\begin{pmatrix} \frac{d_a^{2-2\mu}}{z^{2-2\mu}} & 0 \\ 0 & \frac{d_a^{4-2\eta}}{z^{4-2\eta}} \end{pmatrix} = \frac{z^{2\eta}}{d_a^{2\eta}} \begin{pmatrix} \frac{d_a^2}{z^2} & 0 \\ 0 & \frac{d_a^4}{z^4} \end{pmatrix}.$$

This completes the proof. □

The solution of the Ermakov-Pinney equation (20), see [31, 42], is

$$w = \left(u^1(t) + C^2v^2(t)\right)^{1/2} \tag{21}$$

where the functions $u(t)$ and $v(t)$ are the fundamental solutions of $w'' = 0$ satisfying the initial conditions $u(0) = z_0^{-(1-\eta)}$, $u'(0) = -(1-\eta)z_0^{-(2-\eta)}$ and $v(0) = 0$, $v'(0) = -z_0^{1-\eta}$. Thus, they are given as

$$u(t) = -(1-\eta)z_0^{-(2-\eta)}k_2t + z_0^{-(1-\eta)} \quad \text{and} \quad v(t) = -z_0^{1-\eta}t. \tag{22}$$

7 Phenomenal Plane Geodesics for Resting Eyes

I first solve the geodesics differential equations when the iso-disparity lines are geodesics. These cases involve the metric tensor parameters $\mu = 1$ and $0 \leq \eta \leq 1$. Next I solve the general case of Theorem 1 when $\mu = \eta = (2n-1)/2n$ for $n \geq 1/2$. Finally, I solve the last and only case of non-zero Riemann curvature for the metric tensor parameters $\mu = 0$ and $\eta = 1$.

7.1 Geodesics for $\mu = 1$

The geodesic equations can be solved explicitly when $\mu = 1$ and $0 \leq \eta \leq 1$. The equations (16) and eq:z"g for these parameters can be easily integrated for the initial conditions $(0, z_0)$, $y'(0) = k_1$ and $z'(0) = k_2$, to obtain

$$y'(t) = k_1 \tag{23}$$

and

$$z'(t) = k_2z^{2-\eta}/z_0^{2-\eta}. \tag{24}$$

Next, the unit-speed parametrization of the geodesic: $||(y', z')|| = 1$, for $\mu = 1$ and $0 \leq \eta \leq 1$, gives the condition,

$$g_{yy}y'^2(t) + g_{zz}z'^2(t) = k_1^2 + k_2^2\frac{d_a^{4-2\eta}}{z_0^{4-2\eta}} = 1. \tag{25}$$

where g_{yy} and g_{zz} are given in (12.

The geodesic starting at $(0, z_0)$ in the direction of $(k_1, 0)$ such that, by (25), $k_1 = 1$, is

$$\gamma_1(t) = (t, z_0)$$

and is defined on $(-\infty, \infty)$. This is the iso-disparity line passing through $(0, z_0)$.

The geodesic starting at (y_0, z_0) in the direction of $(0, k_2)$ where again by (25), $k_2 = z_0^{2-\eta}/d_a^{2-\eta}$ can be obtain by a straightforward integration of the equation (24). We need to distinguish two cases.

Case 1: $0 \leq \eta < 1$,

$$\gamma_2(t) = \left(y_0, \frac{z_0}{\left(1 - (1-\eta)\frac{z_0^{1-\eta}}{d_a^{2-\eta}} t\right)^{1/(1-\eta)}} \right),$$

which is defined on the interval $(\xi, d_a^{2-\eta}/((1-\eta)\xi^{1-\eta}))$ for ξ, the closest point on which the eyes can fixate, and $\eta < 1$. The case $\mu = 1$ and $\eta = 1$ will be discussed later. The unit-speed parametrization implies that the parameter t is the arc length. Therefore, solving

$$z(t_1) = z_1 = \frac{z_0}{\left(1 - (1-\eta)\frac{z_0^{1-\eta}}{d_a^{2-\eta}} t_1\right)^{1/(1-\eta)}}$$

for t_1, we obtain the distance in the gaze direction,

$$d(z_0, z_1) = t_1 = \frac{d_a^{2-\eta}}{1-\eta} \frac{1 - (z_0/z_1)^{1-\eta}}{z_0^{1-\eta}}. \tag{26}$$

The finite distance from ξ to the horizon,

$$\lim_{z_1 \to \infty} d(\xi, z_1) = d(\xi, \infty) = \frac{d_a^{2-\eta}}{(1-\eta)\xi^{1-\eta}}, \tag{27}$$

holds for all $0 \leq \eta < 1$. Further, the distance from the horopter to the horizon is

$$d(d_a, \infty) = \frac{d_a}{1-\eta}. \tag{28}$$

Case 2: $\eta = 1$,

$$\gamma_2(t) = \left(y_0, z_0 \exp \frac{t}{d_a} \right)$$

Again, solving $z_1 = z_0 \exp(t_1/d_a)$ for t_1, we have

$$d(z_0, z_1) = t_1 = d_a(\ln z_1 - \ln z_0). \tag{29}$$

and the horizon is infinitely far away.

7.2 Geodesics for $\mu = \eta = (2n-1)/2n$

Here $g_{11} = d_a^{1/n}/z^{1/n}$, $g_{22} = d_a^{(2n+1)/n}/z^{(2n+1)/n}$ and $z = w^{-2n}$. This case follows the solution of the Ermakov-Pinney equation (20), (22). Expressing μ and η by n, the geodesics differential equations are

$$y' = \frac{k_1}{z_0^{1/n}} z^{1/n}$$

and

$$w'' = \frac{1}{4n^2 d_a^2} \frac{k_1^2}{z_0^{2/n}} w^{-3}$$

with the initial conditions

$$w(0) = z_0^{-1/2n} \quad \text{and} \quad w'(0) = -\frac{1}{2n} z_0^{-(2n+1)/2n} k_2.$$

In this case, the fundamental solutions are

$$u(t) = -\frac{1}{2n} z_0^{-(2n+1)/2n} k_2 t + z_0^{-1/2n} \quad \text{and} \quad v(t) = -z_0^{1/2n} t.$$

such that

$$\begin{aligned} w = \left(u^1(t) + C^2 v^2(t)\right)^{1/2} &= z_0^{-1/2n} \left(\left(\frac{k_2}{2n z_0} t - 1 \right)^2 + \frac{k_1^2}{4n^2 d_a^2} t^2 \right)^{1/2} \\ &= z_0^{-1/2n} \left(\frac{k_1^2}{d_a^2} + \frac{k_2^2}{z_0^2} \right)^{-1/2} \left\{ \left[\frac{1}{2n} \left(\frac{k_1^2}{d_a^2} + \frac{k_2^2}{z_0^2} \right) t - \frac{k_2}{z_0} \right]^2 + \frac{k_1^2}{d_a^2} \right\}^{1/2}. \end{aligned}$$

Therefore,

$$z(t) = w^{-2n}(t) = z_0 \left(\frac{k_1^2}{d_a^2} + \frac{k_2^2}{z_0^2} \right)^n \left\{ \left[\frac{1}{2n} \left(\frac{k_1^2}{d_a^2} + \frac{k_2^2}{z_0^2} \right) t - \frac{k_2}{z_0} \right]^2 + \frac{k_1^2}{d_a^2} \right\}^{-n} \tag{30}$$

and

$$y'(t) = \frac{k_1}{z_0^{1/n}} z^{1/n}(t) = k_1 \left(\frac{k_1^2}{d_a^2} + \frac{k_2^2}{z_0^2} \right) \left\{ \left[\frac{1}{2n} \left(\frac{k_1^2}{d_a^2} + \frac{k_2^2}{z_0^2} \right) t - \frac{k_2}{z_0} \right]^2 + \frac{k_1^2}{d_a^2} \right\}^{-1}, \tag{31}$$

which is easily integrated to get

$$y(t) = 2n d_a \arctan \left[\frac{d_a}{2n k_1} \left(\frac{k_1^2}{d_a^2} + \frac{k_2^2}{z_0^2} \right) t - \frac{k_2 d_a}{k_1 z_0} \right] + C \tag{32}$$

We note that

$$z'(t) = -\frac{1}{z_0^{1/n}} \left[\frac{1}{2} \left(\frac{k_1^2}{d_a^2} + \frac{k_2^2}{z_0^2} \right) t - \frac{k_2}{z_0} \right] z^{(n+1)/n}(t) \tag{33}$$

Now, using (31) and (33), the unit-speed parametrization $||(y', z')||_{g_n} = 1$, that is,

$$\frac{d_a^{1/n}}{z^{1/n}(t)} y'^2(t) + \frac{d_a^{(2n+1)/n}}{z^{(2n+1)/n}(t)} z'^2(t) = 1,$$

give the condition

$$\frac{d_a^{1/n}}{z_0^{1/n}} k_1^2 + \frac{d_a^{(2n+1)/n}}{z_0^{(2n+1)/n}} k_2^2 = 1, \tag{34}$$

i.e., $||(k_1, k_2)||_{g_n} = 1$.

Using (34), for the initial conditions,

$$y(0)=0,\ z(0)=z_0\ \text{ and }\ y'(0)=k_1=\frac{z_0^{1/2n}}{d_a^{1/2n}},\ z'(0)=k_2=0, \tag{35}$$

the geodesic is

$$\gamma_1(t)=\left(2nd_a\arctan\frac{1}{2n}\frac{z_0^{1/2n}}{d_a^{(2n+1)/2n}}t, z_0\left(\frac{1}{4n^2}\frac{z_0^{1/n}}{d_a^{(2n+1)/n}}t^2+1\right)^{-n}\right), \tag{36}$$

and for the initial conditions,

$$y(0)=y_0,\ z(0)=z_0\ \text{ and }\ y'(0)=k_1=0,\ z'(0)=k_2=\frac{z_0^{(2n+1)/2n}}{d_a^{(2n+1)/2n}}, \tag{37}$$

$$\gamma_2(t)=\left(y_0, z_0\left(\frac{1}{2n}\frac{z_0^{1/2n}}{d_a^{(2n+1)/2n}}t-1\right)^{-2n}\right). \tag{38}$$

Because t is the arc-length parameter, for the geodesic $\gamma_2(t)$ the distance between (y_0,z_0) and (y_0,z_1) can be easily obtained by solving $\gamma_1(t_1)=z_1$ for t_1,

$$d(z_0,z_1)=t_1=2nd_a^{(2n+1)/2n}\frac{z_1^{1/2n}-z_0^{1/2n}}{z_0^{1/2n}z_1^{1/2n}}. \tag{39}$$

The total length of the geodesic along the gaze line from the point $(0,\xi)$, the closest point that can be fixated binocularly, is

$$d(\xi,\infty)=\frac{2nd_a^{(2n+1)/2n}}{\xi^{1/2n}}=2nd_a\left(\frac{d_a}{\xi}\right)^{1/2n}, \tag{40}$$

meaning that the z-geodesic is incomplete and the total distance to the horizon is finite.

$$d(d_a,\infty)=2nd_a=\frac{d_a}{1-\eta}. \tag{41}$$

Calculus' standard routines show that the minimum value of $d(\xi,\infty)$ is occurring for $n=(1/2)\ln(d_a/\xi)$. Taking $\xi=3$ cm and the average abathic distance of 100 cm, then $n\approx 7/4$ and $\mu=\eta\approx 5/7$. The minimum of $d(\xi,\infty)$ is 953 cm.

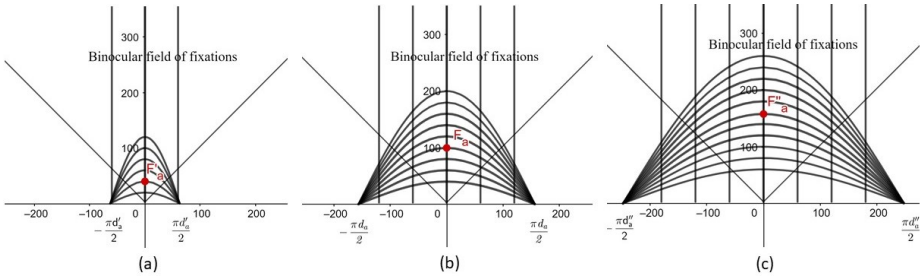

Figure 7: The geodesics in the resting eyes visual space for $n=1/2$. (a) $d_a=40.2$ cm, (b) $d_a=99.61$ cm, and (c) $d_a=157.75$ cm. The curved geodesics start in ∂_y direction from the points $(0,z_0)$. They are extended to the whole interval $(-\infty,\infty)$ and approach asymptotically two points on the y-axis at $\pm(\pi/2)d_a$. The vertical geodesics start in ∂_z direction from the points (y_1,z_0). They are defined on the maximal interval $(0,d_a^2/z_0)$.

The next case does not involve the Ermakov-Pinney equation.

7.3 Geodesics for $\mu = 0$, $\eta = 1$

This is the case of *hyperbolic half-plane with* $g_{yy} = d_a^2/z^2$ *and* $g_{zz} = d_a^2/z^2$. *Here, the geodesic differential equations (16) and (17) are*

$$y'' - \frac{2}{z} y' z' = 0, \tag{42}$$

and

$$z'' + \frac{1}{z} y'^2 - \frac{1}{z} z'^2 = 0. \tag{43}$$

This is a well-known case of the upper-plane model of hyperbolic geometry modified by taking in the metric tensor d_a^2/z^2 *instead of* $1/z^2$. *Assuming* $y' = 0$, *for the initial conditions* $y(0) = y_0$, $z(0) = z_0$, $y'(0) = 0$ *and* $z'(0) = k_2$, *we obtain geodesic*

$$\gamma_1(t) = \left(y_0, z_0 e^{t/d_a} \right).$$

Further, if $y' \neq 0$, *the equation (42) is easily integrated for the initial conditions* $y(0) = y_0$, $z(0) = z_0$, $y'(0) = k_1$ *and* $z'(0) = 0$,

$$y' = \frac{k_1}{z_0^2} z^2 = 0, \tag{44}$$

such that the second equation becomes

$$z'' + \frac{k_1^2}{z_0^4} z^3 - \frac{1}{z} z'^2 = 0. \tag{45}$$

Then, the solutions of (44) and (45) are

$$y(t) = z_0 \frac{e^{2k_1 t/z_0} - 1}{e^{2k_1 t/z_0} + 1} + y_0, \quad \textit{and} \quad z(t) = 2z_0 \frac{e^{k_1 t/z_0}}{e^{2k_1 t/z_0} + 1}.$$

It is easy to check that

$$y'(t) = \frac{k_1}{z_0^2} z^2(t) \quad \textit{and} \quad z'(t) = \frac{k_1}{z_0^2} (y(t) - y_0) z(t).$$

Then, the unit-speed parametrization gives

$$g_{yy} y'^2 + g_{zz} z'^2 = d_a^2 \frac{k_1^2}{z_0^4} \left((y(t) - y_0)^2 + z^2(t) \right) = d_a^2 \frac{k_1^2}{z_0^2} = 1$$

and, therefore, $k_1 = z_0/d_a$.

Thus, the unit-speed geodesics are

$$\gamma_2(t) = \left(z_0 \frac{e^{2t/d_a} - 1}{e^{2t/d_a} + 1} + y_0, 2z_0 \frac{e^{t/d_a}}{e^{2t/d_a} + 1} \right),$$

which represent a family of semicircles in visual space with their centers on the y*-axis at* y_0,

$$(y(t) - y_0)^2 + z^2(t) = z_0^2. \tag{46}$$

In this case, the distance formula is

$$d(z_0, z_1) = d_a (\ln z_1 - \ln z_0)$$

and the horizon is infinitely away.

7.4 Graphs of Geodesic curves

The geodesics are explicitly solved above for the following metric tensor (9) parameters: $\mu = 1, 0 \leq \eta \leq 1$, $\mu = \eta = (2n-1)/2n, n \geq 1/2$, *and* $\mu = 0, \eta = 1$. *In this subsection I compare graphs of typical geodesics for selected values of parameters. These graphs are shown in Figure (8) for the average abathic distance* d_a *of about* 100 *cm.*

In this figure, the vertical lines are geodesics in the Cyclopean gaze direction ∂_z. *They are defined for* $z > \xi$, *where* ξ *expresses anatomical constraints, and are of finite lengths for* $\eta < 1$. *Thus, the horizon is infinitely far away for metrics parameters* $\mu = 1, \eta = 1$ *and* $\mu = 0, \eta = 1$ *discussed in Section 7.1, Case 2 and in Section 7.3, respectively.*

Next, shown in gray color, are geodesics for $\mu = 1, 0 \leq \eta \leq 1$ *starting in the* ∂_y *directions; they agree with the iso-disparity frontal lines. The green curves and blue curves are the geodesics for the cases of* $\mu = 0, \eta = 0$ *and* $\mu = 1/2, \eta = 1/2$, *respectively. We see that when* $(\mu, \eta) \to (1, 1)$, *the geodesics are approaching the iso-disparity lines.*

Finally, the half-circles in brown are the geodesics for $\mu = 0, \eta = 1$ *derived in Section 7.3 for the case of the hyperbolic half-plane. These circles are orthogonal to the* y*-axis. The curvature of the hyperbolic half-plane model is obtained in the next section. All geodesics starting on the* z*-axis in the* ∂_y *direction are extendable to the interval* $(-\infty, \infty)$.

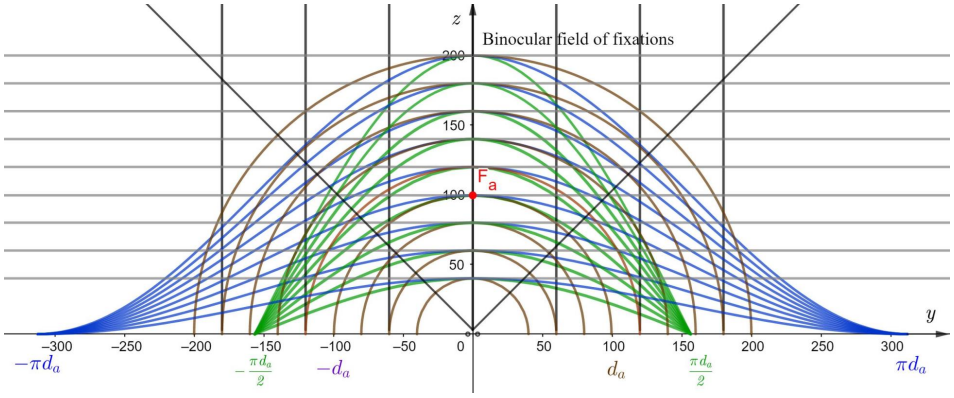

Figure 8: Geodesics in visual plane with the metric tensors (9) for selected parameters. The discussion is given in the text.

8 Curvature

8.1 Geodesic Curvature of Iso-disparity Curves

The iso-disparity curves in physical space are Euclidean lines of constant z*-values. How far this iso-disparity line differs from the geodesic is given by its geodesic curvature. Thus, every geodesic has zero geodesic curvature; see [33]. The unit speed iso-disparity line passing through* $(0, z_0)$ *is* $(y(t), z_0) = ((z_0^{1-\mu}/d_a^{1-\mu})t, z_0)$. *It has the acceleration components*

$$\frac{\nabla y'(t)}{dt} = \Gamma^y_{yy}(z_0)y'(t)y'(t) = 0$$

and

$$\frac{\nabla z'(t)}{dt} = \Gamma^z_{yy}(z_0)y'(t)y'(t) = (1-\mu)\frac{z_0^{1+2\mu-2\eta}}{d_a^{2+2\mu-2\eta}}\frac{z_0^{2-2\mu}}{d_a^{2-2\mu}} = (1-\mu)\frac{z_0^{3-2\eta}}{d_a^{4-2\eta}}.$$

The geodesic curvature of the iso-disparity curve is

$$\kappa = \left\| \left(\frac{\nabla y'(t)}{dt}, \frac{\nabla z'(t)}{dt} \right) \right\| = \sqrt{\frac{d_a^{4-2\eta}}{z_0^{4-2\eta}}(1-\mu)^2\frac{z_0^{6-4\eta}}{d_a^{8-4\eta}}} = |1-\mu|\frac{z_0^{1-\eta}}{d_a^{2-\eta}}. \tag{47}$$

Thus, the iso-disparity line (a Euclidean line) for the resting eyes at the abathic distance d_a that is passing through $(0, z_0)$ is a curve with a non-zero geodesic curvature (47) if and only if $\mu \neq 1$. In particular, the horopteric line, in this case, the horopter has the geodesic curvature $|1-\mu|/d_a$. If $\mu = 1$ and $0 \leq \eta \leq 1$, the iso-disparity lines are geodesics.

8.2 The Riemann Curvature

Here the derivation of the Riemann curvature of visual space is only sketched for the resting eyes, and the reader is referred to Appendix A.4 for a complete introduction to this complicated object. In the basis vectors ∂_i, where the index runs here over y and z, the covariant differentiation ∇_{∂_i} on the basis vectors is

$$\nabla_{\partial_j}\partial_k = \sum_m \Gamma^m_{jk}\partial_m. \tag{48}$$

Following [33], the index notation of the curvature tensor can be written as,

$$\sum_m R^m_{jkl}\partial_m = \nabla_{\partial_j}\nabla_{\partial_l}\partial_k - \nabla_{\partial l}\nabla_{\partial_k}\partial_j,$$

which, in low indices, is the following:

$$R_{ijkl} = \sum_m g_{im}R^m_{jkl}.$$

Using the notation corresponding to coordinates (y, z): (12); (13); (14); (15) and (48), the Riemann curvature tensor can be calculated based on (77) as follows:

$$R_{yzyz} \quad = \quad -\frac{1}{2}g_{yy,zz} + \frac{g^2_{yy,z}}{4g_{yy}} + \frac{g_{yy,z}g_{zz,z}}{4g_{zz}} \tag{49}$$

Further, the scalar curvature is

$$R = 2|g|^{-1}R_{yzyz},$$

where $|g|$ is the determinant of the metric tensor, and the Gaussian curvature is

$$K = \frac{1}{2}R. \tag{50}$$

Substituting,

$$g_{yy,z} = -(2-2\mu)\frac{d_a^{2-2\mu}}{z^{3-2\mu}}, \;\; g_{yy},zz = (2-2\mu)(3-2\mu)\frac{d_a^{2-2\mu}}{z^{4-2\mu}}, \;\; g_{zz},z = -(4-2\eta)\frac{d_a^{4-2\eta}}{z^{5-2\eta}} \tag{51}$$

into (49), we obtain

$$R_{yzyz} = -(1-\mu)(\eta-\mu)\frac{d_a^{2-2\mu}}{z^{4-2\mu}} \tag{52}$$

and

$$K = -(1-\mu)(\eta-\mu)\frac{d_a^{2-2\eta}}{z^{4-2\eta}} \tag{53}$$

We see that when $\mu = 1$ or $\mu = \eta$, the Riemann curvature tensor vanishes identically and visual space is flat [33].

The expression in (53) gives the values of the Gaussian curvature for all parameters of the metric tensor. It is shown in the next figure and discussed in the caption.

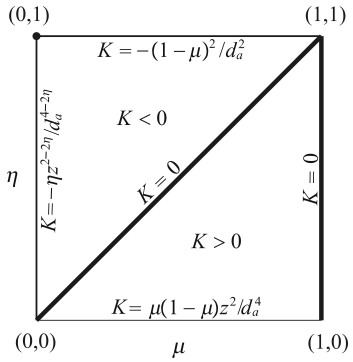

Figure 9: The figure shows the Gaussian curvature for the metric tensor parameters. The Gaussian curvature for solutions on the diagonal and the vertical right side is zero, and all 2D phenomenal spaces are flat. Also, on this vertical side, the iso-disparity lines are geodesics. At the corner $(0, 1)$, the Gaussian curvature is $K = -1/d_a^2$ and the visual space is the hyperbolic half-plane. The explicit geodesics are obtained for the above-discussed subset of parameters. Further, the Gaussian curvature is negative above the diagonal and positive below the diagonal (except on the vertical side where it is zero).

9 Phenomenal Angles in Visual Spaces

9.1 Angles for Metric Tensor g_n

Let $K = (k_1, k_2)$ be the vector at (y_1, z_1) of unit length in visual space with the metric tensor (9) denoted by g_n in the case of $\mu = \eta = (2n - 1)/2n$. Thus, we have

$$||K|| = \frac{d_a^{1/n}}{z_1^{1/n}} k_1^2 + \frac{d_a^{(2n+1)/n}}{z_1^{(2n+1)/n}} k_2^2 = 1. \tag{54}$$

I assume here for simplicity that $k_1 \geq 0$ and $k_2 \geq 0$. Then, for a given two vectors, $V = (1, 0)$ and $V' = (0, 1)$, the angle ψ_n between V and K satisfies the relation

$$\cos\psi_n = \frac{\langle V, K\rangle_{g_n}}{||V||_{g_n}||K||_{g_n}} = \frac{d_a^{1/2n}}{z_1^{1/2n}} k_1$$

and the angle ψ'_n between K and V' satisfies the relation

$$\cos\psi'_n = \frac{\langle K, V'\rangle_{g_n}}{||V||_{g_n}||K||_{g_n}} = \frac{d_a^{(2n+1)/2n}}{z_1^{(2n+1)/2n}} k_2.$$

Thus, the following relation is satisfied,

$$\cos^2\psi_n + \cos^2\psi'_n = 1. \tag{55}$$

Further,

$$\cos(\psi_n + \psi'_n) = \frac{\langle V, V'\rangle_{g_n}}{||V||_{g_n}||V'||_{g_n}} = 0.$$

Clearly, on the basis of the above results, $\psi_n + \psi'_n = \pi/2$ such that $\cos\psi'_n = \sin\psi_n$. Using this last formula, we get the relation between the Euclidean angle φ and visual space angle ψ_n for the metric tensor g_n,

$$\tan\psi_n = \frac{d_a}{z_1}\tan\varphi \tag{56}$$

Thus, the angle ψ_n is independent of n as it should be because all the metrics tensors g_n are conformally equivalent.

However, the angle depends on its position in visual space. If $z_1 = md_a$, then the corresponding angle is $\psi = \arctan((1/m)\tan\varphi)$, and if $z_1 = d_a/m$, then the corresponding angle is $\psi = \arctan(m\tan\varphi)$. The angles ψ in degrees for $\varphi = 30^\circ$ are listed in the left side of Table 1 for the metric tensor g_n.

Table 1: Angles in visual plane. The left table show changes of the angle 30° for metrics g_n as its position is shifted by a multiple of d_a. The right side of the table show changes for the metric g.

	Metric Tensor g_n		Metric Tensor g	
m	ψ at $z_1 = md_a$	ψ at $z_1 = d_a/m$	θ at $z_1 = md_a$	θ at $z_1 = d_a/m$
4	8.213	66.587	2.067	83.822
2	16.102	49.107	8.213	66.587
1.2	25.693	34.715	21.848	39.740
1	30.000	30.000	30.000	30.000

9.2 Angles for the metric with $\mu = 1$ and $\eta = 0$

In this case, the metric is denoted by g, which is not conformally equivalent with g_n metrics. Here the metric element ds is given by $ds^2 = dy^2 + d_a^4/z_1^4 dz^2$. Thus, the unit vector $K = (k_1, k_2)$ in visual space satisfies the relation

$$||K|| = k_1^2 + \frac{d_a^4}{z_1^4}k_2^2 = 1. \tag{57}$$

Similarly as before, the angle θ between V and K is given by

$$\cos\theta = \frac{\langle V, K\rangle_g}{||V||_g||K||_g} = k_1$$

and the angle θ' between K and V' satisfies the relation

$$\cos\theta' = \frac{\langle K, V'\rangle}{||V||_g||K||_g} = \frac{d_a^2}{z_1^2}k_2.$$

Again, θ and θ' are complementary angles such that the relation between Euclidean angle φ and visual space angle θ for the metric g is

$$\tan\theta = \frac{d_a^2}{z_1^2}\tan\varphi. \tag{58}$$

As before, I take $\varphi = 30^\circ$, $z_1 = md_a$ and $z_1 = d_a/m$ to calculate the values of θ. The results are shown in Table 1 on the right for metric tensor g.

9.3 Angles for Hyperbolic metric

The metric in this case is conformally equivalent to Euclidean metric. The angles behave as Euclidean angles, they do not change with the position in visual space.

10 Discussion

In the AEs resting posture, i.e., when they are fixated at the abathic distance in the horizontal field of binocular fixations, the equatorial planes of the eyes' crystalline lenses are coplanar and, hence, the iso-disparity conics are straight frontal lines, cf. Figure 1. The iso-disparity conics consist of families of hyperbolas or ellipses for other horizontal fixations. The abathic distance depends on the AE's parameters α and β; the angle α specifies the fovea's displacement from the posterior pole, and the angle β specifies the lens' tilt relative to the cornea. While the fovea's displacement is the main contribution to the optical aberrations, the lens' tilt cancels some of the optical aberrations by contributing to the human eye's aplanatic design [2].

The resting eyes postures in the horizontal field of binocular fixations define the unique distribution of the iso-disparity frontal lines. Simulations demonstrate this in Figure 2 where two fixations at different abathic distances give the same distribution of the iso-disparity lines. This iso-disparity invariance is the key fact imposed by the AE model that guides the development of the phenomenal metric in the binocular field for the resting eyes.

The simulations of the iso-disparity conics for other than the resting eyes postures are shown in Figures 3 and 4 for the AEs two angles $\beta = 0.5^\circ$ and $\beta = 4^\circ$ that specify the corresponding abathic distances of 40.2 cm and 157.75 cm, respectively. More precisely, in Figure 3, the symmetric fixations are at the same distance of 99.61 cm and are compared to the iso-disparity lines for the fixation also at the abathic distance of 99.61 cm. We see that the spacing of successive conics along the Cyclopean gaze line depends only on the fixation point. However, for asymmetric fixations in Figure 4, the iso-disparity conics also undergo rotations and translations, and their scale changes slightly.

I want to emphasize that the geometric model of the empirical horopters as conic sections constructed in [54] in the binocular system with the AEs advanced the classical model of empirical horopters introduced as conic sections in an ad hoc way by Ogle in [39]. This theory is extended here to iso-disparity conic sections. Thus, this extension provides the first-ever iso-disparity curves integrated with eye movements in the horizontal binocular field of fixation. The lack of the construction of a family of iso-disparity curves that would more richly describe the structure of binocular visual space was mentioned in [1].

I assume that the distance between successive iso-disparity lines for a constant disparity is the veridically perceived depth at the abathic distance fixation. This seems to be a natural assumption, especially since the distribution of the iso-disparity lines is abathic-distance invariant. Because disparity is here considered the only cue the brain is using to gauge depth, its constant value at different egocentric distances determined by disparity requires that physical space is expanded between the head and the horopter and contracted beyond the horopter. The visual space global aspects of geometry for eyes resting posture are shaped by these phenomenal deformations of the binocular field of fixations.

The Riemannian geometry framework determines visual space spatial relations by the Riemann metric tensor. I recall that because of the absence of a theory that can specify the depth perception from the biological architecture of the visual system; I postulate a two-parameter family of metric tensors for the resting eyes postures, that is, for fixations at the abathic distance d_a, as follows:

$$\begin{pmatrix} \frac{d_a^{2-2\mu}}{z^{2-2\mu}} & 0 \\ 0 & \frac{d_a^{4-2\eta}}{z^{4-2\eta}}, \end{pmatrix} \tag{59}$$

where $0 \leq \mu \leq 1$, and $0 \leq \eta \leq 1$.

This section discusses the implications of the parameters' values for the global aspects of phenomenal geometry and their relation to other studies. To this end, I first list in Table 2 the representative properties for selected values of μ and η obtained in the previous sections. These properties include the distance to the horizon for the average abathic distance d_a of about 100 cm and the anatomic constraint of $\xi = 3$ cm for the shortest distance at which eyes can fixate; the Gaussian curvature of the phenomenal binocular plane; and the geodesic curvature of the iso-disparity lines which tales how far the iso-disparity (Euclidean) lines differ from being geodesics.

Table 2: The properties of the geodesics for the metric tensors listed in the first column.

Global Geometry of 2D Visual Space					
Metric Tensor with μ, η	Conformally Equivalent	Distance to the Horizon*	Gaussian Curvature K	Are IDLs Geodesic	z_0-IDL Geodesic Curvature κ
$0,\ 0$	Yes	3333 cm	0	No	z_0/d_a^2
$1/4,\ 1/4$	Yes	1850 cm	0	No	$3z_0^{3/4}/4d_a^{7/4}$
$1/2,\ 1/2$	Yes	1155 cm	0	No	$z_0^{1/2}/2d_a^{3/2}$
$3/4,\ 3/4$	Yes	961 cm	0	No	$z_0^{1/4}/4d_a^{5/4}$
$1,\ 1$	Yes	infinite	0	Yes	0
$1,\ 0$	No	3333 cm	0	Yes	0
$0,\ 1$	No	infinite	$-1/d_a^2$	No	$1/d_a$
* $d_a = 100$ cm, $\xi = 3$ cm IDLs = Iso-disparity lines z_0-IDL = Iso-disparity line through z_0					

The iso-disparity line through $(0, z_0)$ for fixation at the abathic distance d_a has a non-zero geodesic curvatures whenever $\eta \neq 1$ in (59). Thus, the iso-disparity lines are geodesics only for $\eta = 1$. Otherwise, the geodesics starting at $(0, z_0)$ in direction ∂_y consists of families of curves such that for each of abathic distances d_a the corresponding family

curves asymptotically converge to two points $\pm(n\pi d_a, 0)$ *on the y-axis when* $\mu = \eta = (2n-1)/2n$, $n \geq 1/2$, *cf. (32). Moreover, for* $\mu = 0$ *and* $\eta = 1$, *the geodesics are half-circles approaching perpendicularly the y-axis. Typical geodesics for selected values of parameters are shown in Figure (8) for the average abathic distance* d_a *of about* 100 *cm.*

The distance to the horizon for the average abathic distance of about 100 *m given by geodesics starting at a distance* $\xi = 3$ *cm in the* ∂_z *direction ranges from the minimum value of* 9.5 *m for* $\mu = \eta \approx 5/7$ *to* 33 *m for incomplete geodesics. For two cases of parameters,* $\mu = 1$, $\eta = 1$ *and* $\mu = 0$ *and* $\eta = 1$ *the horizon is infinitely away. The distance from the horopter to the horizon in the gaze direction is* $d_a/(1-\eta)$ *where I assumed that* $0 \leq \eta < 1$. *When* $\eta = 1$, *the distance from the horopter to the horizon is infinite.*

The finite distance to the horizon should be expected as we perceive objects in the horizontal binocular field against the horizon with the depth perception resulting from the metric (7) such that our field of vision appears two-dimensional with the objects perceived to be located in the initial visual processing at different distances from the horopter and finally perceived distributed relative to each other in the egocentric coordinates. This relative location of the objects contributes to phenomenal geometry.

In literature, the distance of the vanishing points at the horizon is reported to be between 6 *m and* 100 *m in some studies or even ranging from* 100 *cm to infinity in other studies, see [15]. Here, the AE model in the binocular system determines the eyes' resting vergence posture abathic distance that depends on the lens tilt angle* β. *The simulations are carried out for three values of the abathic distances;* $d_a(0.5^\circ) = 40.2$ *cm,* $d_a(3.3^\circ) = 99.61.$ *cm, and* $d_a(4^\circ) = 157.75$ *cm. For these values, I obtain the distance to the horizon* 5.4 *m,* 33 *m, and* 83 *m, respectively, for the metric tensor's parameters* $\mu = 0$ *and* $\eta = 0$. *For parameters* $\mu = 1$, $\eta = 1$ *and* $\mu = 1$, $\eta = 1$ *the horizon is infinitely away. These results suggest experiments to test the relation between perceived distance to the horizon, the eye's tilt, and the visual metric parameters in a people population.*

The curvature of the horizontal visual set, derived here for the eyes' resting posture when they fixate at the abathic distance d_a, *is zero. Hence, the visual plane is flat for the subset of the metric tensors (59) parameters shown in Figure 9. This subset consists of the diagonal* $\mu = \eta$ *with geodesics derived by transforming the geodesic differential equations to the Ermakov-Pinney equations (Theorem 1), and the left vertical side* $\mu = 1$ *with geodesics derived directly. At the corner* $\mu = 0$ *and* $\eta = 1$ *when the visual plane geometry corresponds to the half-plane model of hyperbolic plane with the Gaussian curvature* $-1/d_a^2$. *Moreover, the Gaussian curvature for the eyes' resting posture is known for the whole range of parameters assumed for the metric tensor (59); see Figure 9.*

How do the results obtained in this article relate to other studies in spatial perception? I need to mention two principal assumptions guiding this research to discuss it. First, the phenomenal geometry is restricted to binocular disparity-based stereopsis. Second, the study of phenomenal space in the Riemannian geometry framework is also supported by the eye's anatomy and retinal photoreceptors' topography. Thus, the psychological processes that are important in the multi-cue spatial perception and the related psychophysical line of studies are not considered here.

Reid developed in [44] an informal spherical geometry of visual space that is perceived by a single eye. Reid assumed that the retina's shape was spherical and placed the eye at the center of a large sphere. Then, every visible figure is represented by its projection into the sphere. Thus, great circles represent straight lines. Reid concluded that there are no parallel lines since any two great circles interest at two antipodal points. He also pointed out that the sum of the internal angles of a triangle will appear greater than 180° *exactly as in its projection into the sphere. Critically, Reid's geometry supports only a monocular vision.*

Helmholtz was the first to realize that the visual space geometry should be one of the constant curvature geometries: Euclidean, elliptic or hyperbolic; see the collection of Helmholtz' Epistemological Writings [22]. Helmholtz came to this conclusion after he investigated the most general axioms of geometry for which the spatial properties of figures to be preserved under his 'rigid motions' such that objects' measurement processes are possible. Further, Helmholtz investigated in much detail the question of how non-Euclidean geometries can be visualized. However, he concluded that their impact on visual space should be left to experimental investigations.

Luneburg, in his classical mathematical works in psychology of vision [34, 35, 36] used two experiments performed in dark rooms with luminous points. In the first experiment, Helmholtz arranged lines that appeared fronto-parallel but were objectively curved. In the second experiment, Blumenfeld arranged two pairs of alleys: the first that appeared with parallel lines (the original Hillebrand's experiment) and the second that appeared equidistant. In contradiction to Euclidean geometry, the apparently parallel alley was inside the apparently equidistant alley. Based on the experiments results, Luneburg concluded that visual space geometry is hyperbolic. His theory was further developed most notably by Blank [7, 8, 9] and by Indow [25, 26].

Subsequently, many axioms underlying Luneburg theory, including Helmholtz's mobility condition, were called into question; please refer to Wagner [59] for detailed discussion. Nevertheless, none of the many attempts to modify Luneburg's theory have been successful.

Moreover, Battro et al. in [5] repeated Luneburg's measurements in photopic conditions and with different sizes of equidistant and parallel alleys. The curvature was obtained, ranging from negative to positive and subject-dependent. Also, Schelling in [47] noticed that the hyperbolic metric should be specified relative to the fixation point such that the theory needs to be extended because eyes are constantly moving. Further, based on results in [16, 58], Suppes in [51] noticed that most likely different geometries are required because the spatial relations in phenomenal space are dependent on performed experimental tasks. Finally, Koenderink et al. [29, 30] used triangle adjustment to determine that the curvature of visual space was positive for near stimuli and negative for distant stimuli. For very large distances, the visual plane became Euclidean.

Beyond the studies mentioned above that employed the axiom-based geometries and their modification attempts, phenomenal geometries were also studied based on methods of analytic geometry. These methods include a set of coordinates assigned to a space, and equations are developed to model the measurable properties of the space, such as distances and angles, while also including stimulus location in physical space and psychological factors. A general form of analytic geometry is the theory of metric spaces. For thorough discussions of this line of studies, usually supported by psychophysical methods (numeric and category estimates or sensitivity measures, for example), the reader is directed to [59].

10.1 Concluding Remarks

Julesz's random-dot stereogram [28] confirmed Wheatstone's observation made in [61] that the brain uses binocular disparity to determine the relative distance of different parts of a solid object to sense its shape, that is, stereopsis. More importantly, it asserted that the spatial relations in visual space could be separated from psychological processes. This realization laid the ground for studies in the physiology basis of stereopsis, cf. [24, 3, 43] and many others. Here, phenomenal space global geometry is studied using binocular disparity alone.

The theory used here for modeling phenomenal space is based on the framework of Riemannian geometry, with the metric tensor being its fundamental concept. However, in contrast to the psychophysical line of investigations of the geometric relations in spatial vision, the phenomenal metric is proposed here using geometric simulations and numerical methods coupled with the eye anatomy and photoreceptors' topography. In general, I believe that psychophysical studies neglect possible insights gained from anatomical architecture underlying physiological vision processes. The chief example is the horopter's concept: anatomically incorrect, 200-year-old the Vieth-Müller circle as the geometric horopter has been only recently corrected in the two geometric theories with progressively higher eye model anatomic fidelity [52, 54].

I conclude this section by pointing to future research directions. First, considering the metric tensor as a two-parameter family results from the lack of a theory that can describe how relative depth and size vary with disparity and distance based on the architecture of the visual system and related physiological processes. It shows the direction for the experimental studies of the two-parameter set of metrics. Second, in the cases of the hyperbolic and elliptic iso-disparity families, the metric tensor will depend on both the y and z coordinates. Even if these conics are geodesics, what could be the case if the iso-disparity frontal lines for the resting eyes are geodesics, the metric may not be derived from unparametrized geodesics, see [10]. The sign of the phenomenal curvature can be inferred from the conics, the minus sign for the diverging hyperbolic geodesics, and the plus sign for the converging elliptic geodesics. These issues should be studied in the future.

APPENDIX

A Riemannian Geometry Primer

The binocular space of fixations, B, is a convex subset in the horizontal visual plane discussed in Section 3. The global coordinate system (x^i) is specified relative to the stationary upright head where the index i runs over y and z. The coordinates (x^i) give the basis vectors ∂_i introduced in Section 5. The metric tensor $g(\partial_i, \partial_j) = g_{ij}$ on B is obtained from the geometric analysis of disparity-based perception. It define the length of the tangent vector and the angle between two tangent vectors as discussed in Section 5. To avoid technicalities, I review here the basic notions of Riemannian geometry in one global chart. Also I use so called Einstein summation convention*: when an index occurs twice in the same expression in upper and in lower positions, then the expression is implicitly summed over all possible values for that index.*

A.1 Tangent Vectors and Metric

Let $\varphi : M \to R^n$, $\varphi(p) = (x^i)$, be a global chart on a manifold M of dimension n. The tangent vector X_p at $p \in M$ is identified with the directional derivative on $f \in C^\infty(M)$ viz.

$$\mathbf{X}_p(f) = X^i \partial_i f(\varphi^{-1})(x^j), \tag{60}$$

where $\partial_i = \partial/\partial x^i$ are partial derivatives. Thus, this tangent vector at p, is $\mathbf{X}_p = X^i \partial_i|_{(p)}$. The set $(\partial_1, \partial_2, ..., \partial_n)$ gives vector basis of the tangent space T_pM of M at p. The tangent space T_pM is identified with R^n that has the origin at p. The tangent vector field on M is a map $\mathbf{X}$ on M such that $\mathbf{X}(p) = \mathbf{X}_p$.

Riemannian space *is a manifold M equipped with a* Riemannian metric *g that for each $p \in M$ defines the scalar product g_p in the tangent space T_pM that depends smoothly on p. For any vector $\mathbf{X} \in T_pM$, $g_p(\mathbf{X}, \mathbf{X})$ defines the square of the length of $\mathbf{X}$. In the basis ∂_i in T_pM, $g_p(\partial_i, \partial_j) = g_{ij}$. Then, for any two vectors $\mathbf{X} = X^i\partial_i$ and $\mathbf{Y} = Y^i\partial_i$ in T_pM, $g_p(\mathbf{X}, \mathbf{Y}) = g_{ij}X^iY^j$.*

A.2 Covariant Derivative and Connection

For a given tangent vector field $\mathbf{X} = X^i\partial_i$, the covariant derivative $\nabla_{\mathbf{X}}$ on a function f on M is defined as the directional derivative

$$\nabla_{\mathbf{X}} f = X^i \partial_i f. \tag{61}$$

To obtain the covariant derivative of a vector field $\mathbf{Y} = Y^i\partial_i$ along $\mathbf{X} = X^i\partial_i$, the previous differentiation is extended as follows

$$\begin{aligned}\nabla_{\mathbf{X}}\mathbf{Y} = \nabla_{X^i\partial_i}(Y^k\partial_k) &= X^i\partial_i(Y^k)\partial_k + Y^k\nabla_{\partial_i}\partial_k \\ &= X^i\partial_i(Y^k)\partial_k + Y^k\Gamma^m_{ik}\partial_m.\end{aligned}$$

where in the last equality the vector field $\nabla_{\partial_i}\partial_k$ is decomposed in the basis ∂_i:

$$\nabla_{\partial_i}\partial_k = \Gamma^m_{ik}\partial_m. \tag{62}$$

The coefficients Γ^m_{ik} are known as Christoffel symbols in the coordinates (x^i).

$\nabla_{\partial_i}\partial_k$ can be interpreted as comparison of vectors ∂_k in infinitesimally close tangent spaces in the direction of ∂_i. Thus, the covariant derivative establishes connection ∇ *between tangent spaces, cf. the discussion in Section 6. Recall that the formulation here is global such that I do not discuss the local aspects of the covariant derivative.*

A connection ∇ is symmetric if

$$\nabla_{\mathbf{X}}\mathbf{Y} - \nabla_{\mathbf{Y}}\mathbf{X} - [\mathbf{X}, \mathbf{Y}] = 0 \tag{63}$$

where $[\mathbf{X}, \mathbf{Y}]$ is the commutator: $[\mathbf{X}, \mathbf{Y}]f = \mathbf{X}\mathbf{Y}f - \mathbf{Y}\mathbf{X}f$. Because in the basis ∂_i, $[\partial_i, \partial_j] = 0$, then we have

$$\nabla_{\partial_i}\partial_k - \nabla_{\partial_k}\partial_i = \Gamma^m_{ik}\partial_m - \Gamma^m_{ki}\partial_m = 0 \tag{64}$$

and, therefore, Christoffel symbols are symmetric $\Gamma^m_{ik} = \Gamma^m_{ki}$ in lower indices.

A symmetric connection is Levi-Civita connection *if it preserves the metric: for any two vector fields $\mathbf{Y}, \mathbf{Z}$,*

$$\nabla_{\mathbf{x}} g(\mathbf{Y}, \mathbf{Z}) = g(\nabla_{\mathbf{X}}\mathbf{Y}, \mathbf{Z}) + g(\mathbf{Y}, \nabla_{\mathbf{X}}\mathbf{Z}) \tag{65}$$

I state the following theorem without proving it.

Theorem 2. *There exists unique Levi-Civita connection on the Riemannian manifold (M, g). In local coordinates Christoffel symbols of Levi-Civita connection are given by*

$$\Gamma^i_{mk} = \frac{1}{2}g^{ij}(g_{jm,k} + g_{jk,m} - g_{mk,j} \tag{66}$$

where (g_{ij}) is the Riemannian metric and (g^{ij}) is the inverse of (g_{ij}).

A.3 Parallel Transport and Geodesics

Let $\mathbf{X}(t)$ be a vector field along a curve $C: x(t) = (x^i(t)), t_0 \leq t \leq t_1$ and $\mathbf{v} = dx(t/dt = dx^i(t)/dt\partial_i|_{x(t)}$ the velocity vector of C. We say that $\mathbf{X}(t)$ is a parallel transport of $\mathbf{X} = \mathbf{X}(t_0)$ along C if the covariant derivative along C is zero

$$\frac{\nabla \mathbf{X}(t)}{dt} = \nabla_{\mathbf{v}} \mathbf{X}(t) = 0 \tag{67}$$

In coordinates, it can be written as

$$\frac{\nabla X^m(t)}{dt} = \frac{dX^m(t)}{dt} + v^i \Gamma^m_{ik}(x^j(t) X^k(t) = 0 \tag{68}$$

Because ∇ is Levi-Civita connection, it is easy to show that the Riemannian metric is preserved *during the parallel transport.*

A parametrized curve $C: x^i(t)$ is geodesic if parallel transport of velocity vector $v^i(t) = dx^i(t)/dt$ along the curve C is a velocity vector at any point of C, that is, if

$$\frac{dv^m(t)}{dt} + v^i(t)\Gamma^m_{ik}(x^j(t))v^k(t) = 0 \tag{69}$$

i.e.,

$$\frac{d^2x^m(t)}{dt^2} + \frac{x^i(t)}{dt}\Gamma^m_{ik}(x^j(t))\frac{x^k(t)}{dt} = 0 \tag{70}$$

Because Levi-Civita connection preserves the Riemannian metric, the length of velocity vector is constant along the geodesic. The geodesic that has unit speed is parametrized by the geodesic's arc length.

A.4 Riemann Curvature Tensor

Coordinate-invariant definition of the Riemann curvature tensor for Levi-Civita connection ∇ is given as

$$\mathcal{R}(\mathbf{X}, \mathbf{Y})\mathbf{Z} = (\nabla_{\mathbf{X}}\nabla_{\mathbf{Y}} - \nabla_{\mathbf{Y}}\nabla_{\mathbf{X}} - \nabla_{[\mathbf{X},\mathbf{Y}]})\mathbf{Z}, \tag{71}$$

where $\mathbf{X}$, $\mathbf{Y}$ and $\mathbf{Z}$ are vector fields. It is a complicated object and I introduce it briefly. In coordinates, the components of the curvature tensor are obtained as follows

$$\mathcal{R}(\mathbf{X}, \mathbf{Y})\mathbf{Z} = \mathcal{R}(X^m\partial_m, Y^n\partial_n)Z^r\partial_r = Z^r R^i_{rmn} X^m Y^n \partial_i \tag{72}$$

where

$$R^i_{rmn}\partial_i = \mathcal{R}(\partial_m, \partial_n)\partial_r$$

Following [33], using that $[\partial_i, \partial_j] = 0$, in the vector basis ∂_i the index notation of the curvature tensor is given by

$$R^i_{kmn}\partial_i = R(\partial_m, \partial_n)\partial_k = \nabla_{\partial_m}\nabla_{\partial_n}\partial_k - \nabla_{\partial_n}\nabla_{\partial_m}\partial_k, \tag{73}$$

which, by substituting $\nabla_m\partial_n = \Gamma^k_{mn}\partial_k$, can be written as

$$R^i_{kmn} = \Gamma^i_{nk,m} + \Gamma^i_{mj}\Gamma^j_{nk} - \Gamma^i_{mk,n} - \Gamma^i_{nj}\Gamma^j_{mk}. \tag{74}$$

in terms of the Christoffel symbols. Then, the Riemann curvature tensor with low indices is

$$R_{ijkl} = g_{im}R^m_{jkl} = (1/2)(g_{il,jk} + g_{jk,il} - g_{ik,jl} - g_{jl,ik}) + g_{pq}(\Gamma^p_{il}\Gamma^q_{jk} - \Gamma^p_{ik}\Gamma^q_{jl}). \tag{75}$$

Now, the curvature tensor for Levi-Civita connection obeys the following identities

$$R_{ikmn} = -R_{ikmn}, \quad R_{ikmn} = -R_{kimn}, \quad R_{ikmn} = R_{mnki}. \tag{76}$$

For two-dimensional Riemannian manifolds these identities imply that R_{1212} yields all components up to a sign. Thus,

$$R_{1212} = (1/2)(g_{12,21} + g_{21,12} - g_{11,22} - g_{22,11}) + g_{pq}(\Gamma^p_{12}\Gamma^q_{21} - \Gamma^p_{11}\Gamma^q_{22}). \tag{77}$$

B The Horopter: Old and New

A group of scientists with extensive teaching records of both normal and abnormal binocular vision that involved both the underlying theory and its multitude of clinical applications described in [12] their experience as follows:

> *A question that has been posed to us on more than one occasion, frequently with a look ranging from inquisitiveness to disdain, is, "Why the horopter?" Certainly, this is a fair question. Unfortunately, the horopter seems to be misunderstood by many, and hence the question.*

Of course, as the next quotation illustrates, some publications contributed to this open contempt for the horopter. It was written in [46],

> *The significance of the horopter [...] has probably been exaggerated. Not only is its physiological significance obscure, but even its psychophysical definition has become ambiguous.*

The horopter's history may partly be responsible for today's ambiguous psychophysical definitions and obscured physiological significance. For a long time, two ideas prevailed about the horopter. The historically first idea, more than 200-year old, introduced independently by Vieth (1818) and Müller (1826), was strictly geometric. It asserted that each point of the horopter in the horizontal plane projects to a pair of corresponding elements, each in one of the two retinas, assuming that the corresponding elements coincide when the retinas are superimposed. This definition of the corresponding elements gives the constant value of the subtended angle at the fixated points along the horopter. Euclid's theorem implies that the horopter is a circle. It is known as the Vieth-Müller circle (VMC).

The second idea was based on the actual experimental determination of the horizontal horopter, which was made first by Hillebrand about 130 years ago, although not by the nonius method described in Section 1; see [48]. Each idea gave different horopter curves, and the empirical horopter is commonly described as 'deviating' from the VMC. However, the empirically measured distribution of the corresponding elements differs between people and is not readily achieved [57], so the geometric idea prevailed even though the precise form of the geometric horopter was not known in general, as is explained below.

In the geometrical description of the horopter, the center of the projection from the VMC to the retina should be placed at the nodal point of a single refractive surface schematic eye model. I recall that the nodal point is distinguished by the property that when the light ray is directed at the point, it passes the eye's optical system without changing its direction. However, the center of projection has not been precisely specified throughout history: Vieth placed it at the pupil and Müller at the lens center. However, the projection center is most often placed at the eye's rotation center, as originally proposed by Volkmann (1836). Only in this last case, when the VMC remains stationary when the eyes' fixation point moves along the circle, its analytic form has been known for all fixations. Otherwise, when the nodal points are in their correct anatomical locations about 0.6 cm anterior to the rotation center [19], the geometric horopter's analytic form has been known only for symmetric fixations.

The analytic form of the geometric horopter for the nodal points located according to the eye's anatomy has been fully known for all fixations only after 2016 work in [52]. More significantly, the geometric model of the empirical horopters as conic sections constructed in [54] in the binocular system with the AEs advanced the classical model of empirical horopters introduced as conic sections in an ad hoc way by Ogle in [39]. In contrast to Ogle's theory, horopters in [54] are anatomically supported, correctly pass through the nodal points, and vary with the AEs' position in the horizontal plane of bifoveal fixations. Their transformations are visualized in a computer simulation.

The geometric theory in [54] is extended here to the iso-disparity conic sections motivated by the eye's anatomy and integrated with eye movements in the horizontal binocular field of fixation. The lack of the construction of a family of iso-disparity curves that would more richly describe the structure of binocular visual space was mentioned in [1].

References

[1] A. Arditi, Binocular Vision, Chapter 23 In Handbook of Perception and Human Performance. Baff, K., Kaufman, L. and Thomas J. (eds.) John Wiley and Sons, 23-1-23-41 (1986).

[2] P. Artal, Optics of the eyes and its impact in vision, Adv. Opt. Photon, 6, 340-367 (2014).

[3] H.B. Barlow, C. Blakemore and J.D. Pettigrew, The Neural Mechanism of Binocular Depth Discrimination, J. Physiol., 193, 327 (1967).

[4] S.R. Barry, Beyond the critical period. Acquiring stereopsis in adulthood. In Plasticity in Sensory Systems. Steeves J.K. and Harris L.R. (eds.). Cambridge University Press. 175-195 (2013).

[5] A.M. Battro, S. di Pierro Netto and R.J.A. Rozenstrafen, Riemannian geometries of variable curvature in visual space: Visual alleys, horopters, and triangles in big open fields. Perception, 5, 9–23 (1976).

[6] C. Blakemore, The Range and Scope of Binocular Depth Discrimination in Man. J. Physiol. 211, 599-622 (1970).

[7] A.A. Blank, The Luneburg theory of binocular visual space, J. Opt. Soc. Am., 43, 717-727 (1953).

[8] A.A. Blank, The geometry of vision. Br. J. Physiol. Opt., 14, 1–30 (1957).

[9] A.A. Blank, Analysis of experiments in binocular space perception, J. Opt. Soc. Am., 48, 911–925 (1958).

[10] K. Burns, V.S. Matveev, Open problems and questions about geodesics, Ergod. Theory Dyn. Syst., 41, 641-684 (2021).

[11] T. Carney, S. A. Klein, Resolution acuity is better than vernier acuity, Vision Res., 37, 525–539 (1997).

[12] K. Ciuffreda, D. Ludlam, B. Tannen and N. Yadav, Brock string and the horopter: A perspective. Vision Dev. and Rehab., 2, 208-210 (2016).

[13] M.P. Do Carmo, Riemannian Geometry, Birkhäuser, Boston 1993.

[14] S.M. Ebenholtz, Oculomotor Systems and Perception, Cambridge U Press 2001.

[15] C.J. Erkelens, Perspective space as a model for distance and size perception, i-Perception, 1-20 (2017).

[16] J.M. Foley, The size–distance relation and intrinsic geometry of visual space: Implications for processing. Vision Res., 13, 323–332 (1972).

[17] P. Ermakov, Second Order Differential Equations. Conditions of Complete Integrability, Universita Izvestia Kiev 9, 1–25 (1880). (Russian).

[18] D. Guitton, M. Volle, Gaze control in humans: eye-head coordination during orienting movements to targets within and beyond the oculomotor range, J. Neurophysiol., 58, 427-459 (1987).

[19] W.L. Gulick and R.B. Lawson, Human stereopsis: A psychophysical analysis. New York: Oxford University Press 1976.

[20] G. Hatfield, Geometry and visual space from antiquity to the early moderns. pp 184-222, In Space: A History. Ed. A. Janiak, New York: Oxford University Press 2020.

[21] H.L.F. Helmholtz, Physiological Optics (J. P. C. Southhall, trans.). Rochester, NY: Optical Society of America 1867/1925.

[22] P. Hertz and M. Schlick, Hermann von Helmholtz Epistemological Writings. Translation of 1921 ed. by M. Love in Boston Studies in Philosophy of Science Vol. XXXVII, R.S. Cohen and Y. Elkana (eds.) D. Reidel Publ. Comp. 1977.

[23] I.P. Howard, B.J. Rogers, Binocular Vision and Stereopsis, Oxford University Press 1995.

[24] D.H. Hubel and T.N. Wiesel, Receptive fields, binocular interactions and functional architecture in the cat's visual cortex, J. Physiol., 160, 106-154 (1962).

[25] T. Indow, A critical review of Luneburg's Model with regard to global structure of visual space, Psychol. Rev., 98, 430-453 (1991).

[26] T. Indow, Hyperbolic representation of global structure of visual space, J. Math. Psychol., 41, 89–98 (1997).

[27] W. Jaschinski-Kruza, Eyestrain in VDU users: viewing distance and the resting position of ocular muscles, Hum. Factors, 33, 69-83 (1991).

[28] B. Julesz, Binocular depth perception without familiarity cues, Scince, 145, 356-362 (1964).

[29] J.J. Koenderink, A.J. van Doom, J. S. Lappin, Direct measurement of the curvature of visual space, Perception, 29, 69-79 (2000).

[30] J.J. Koenderink, A.J. van Doorn and J.S. Lappin, Exocentric pointing to opposite targets. Acta Psychol. (Amst), 112, 71–87 (2003).

[31] P. Korman, A remark on Pinney's equation, arXiv:1902.02739v1 [mathAP], 1-2 (2019).

[32] P.G.L. Leach, K. Andriopoulos, The Ermakov Equation: A Commentary, Appl. Anal. Discrete Math., 2, 146-157 (2008).

[33] J.M. Lee, Riemannian Manifolds: An Introducton to Curvature, Springer 1997.

[34] R.K. Luneburg, Mathematical Analysis of Binocular Vision, Princeton University Press 1947.

[35] R.K. Luneburg, Metric methods in binocular visual perception, In Courant Anniversary Volume, New York: Interscience, 215-240 (1948).

[36] R.K. Luneburg, The metric of visual space. J. Opt. Soc. Am., 40, 627–642 (1950).

[37] G. Maiello, M. Chessa, P.J. Bex, F. Solari, Near optimal combination of disparity across a log-polar scaled visual field, PLoS Comp. Biol., 16(4):e1007699 (2020).

[38] A.M. Norcia, E.E. Sutter, C.W. Tyler, Electrophysiological evidence for the existence of coarse and fine disparity mechanisms in human, Vision Res., 25, 1603-1611 (1985).

[39] K.N. Ogle, An analytical treatment of the longitudinal horopter; its measurement and application to related phenomena, especially to the relative size and shape of the ocular images, J. Opt. Soc. Am., 22, 665-728, (1932).

[40] K. Ogle, Researches in Binocular Vision, PA:WB Saunders, Philadelphia 1950.

[41] K. N. Ogle, Precision and validity of stereoscopic depth perception from double image, J. Opt. Soc. Am. 41, 906–913 (1953).

[42] E. Pinney, The nonlinear differential equation $y'' + p(x)y + cy^{-3}$, Proc. Am. Math. Sc. 1, 681 (1950).

[43] G.F. Poggio and W.H. Talbot, Neural mechanisms of static and dynamic stereopsis in foveal cortex of rhesus monkey. J. Physiol., 315, 469-492 (1981).

[44] T. Reid, An Inquiry into the Human Mind on the Principles of Common Sense. In: The Works of Thomas Reid, W. Hamilton (ed.), Edinburgh: MacLachlan and Stewart, pp. 93–211 (1764/1852).

[45] J.C.A. Read, The place of human psychophysics in modern neuroscience, Neuroscience, 296, 116-129 (2014).

[46] W. Richards, Visual space perception. Vol. V. In: Handbook of Perception, C. Carterette, M.P. Friedman (eds.), New York: Academic Press 1975.

[47] H. Schelling, Concept of distance in affine geometries and its applications in theories of vision, . J. Opt. Soc. Am., 46, 309-315 (1956).

[48] T. Shipley, S. Rawlings, The Nonius Horopter-I. History and Theory, Vision Res., 10. 1225–1262 (1970).

[49] T. Shipley and S. Rawlings, The Nonius Horopter–II. An Experimental Report, Vision Res., 10, 1263-1299 (1970).

[50] P. Suppes, Is visual space Euclidean? Synthese, 35, 397-421 (1977).

[51] P. Suppes, Some foundational problems in the theory of visual space. In Geometric representations of perceptual phenomena, R. D. Luce, M. D'Zmura, D. Hoffman, G. J. Iverson, A. K. Romney (Eds.) Mahwah, NJ: Lawrence Erlbaum Associates. 37-45 (1995).

[52] J. Turski, On binocular vision: the geometric horopter and cyclopean eye, Vision Res., 119, 73–81 (2016).

[53] J. Turski, Binocular system with asymmetric eyes, J. Opt. Soc. Am. A 35, 1180-1191 (2018).

[54] J. Turski, A geometric theory integrating human binocular vision with eye movement, Front. Neurosci. 14:555965, 1-17 (2020).

[55] J. Turski, On Riemannian Geometries of Visual Space, BioRxiv, Version 3, 1-10 (2021).

[56] C.W. Tyler, Binocular vision. Vol. 2 In W. Tasman and E. A. Jaeger (Eds.). Duane's foundations of clinical ophthalmology, Philadelphia: J.B. Lippincott 2004.

[57] G. von Noorden and E.C. Campos, Binocular Vision and Ocular Motility: Theory and Management of Strabismus. Mosby, A Harcourt Health Sciences Company, St. Louis 2002.

[58] M. Wagner, The metric of visual space. Percept Psychophys, 38, 483–495 (1985).

[59] M. Wagner, The Geometries of Visual Space, Lawrence Erlbaum Associates, Mahwah, NJ 2006.

[60] G. Westheimer, The ferrier lecture, 1992. seeing depth with two eyes: stereopsis, Proc. R. Soc. Lond. B, 257, 205-214 (1994).

[61] C. Wheatstone, Contributions to the physiology of vision—Part the first. On some remarkable and hitherto unobserved phenomena of binocular vision. Philos. Trans. R. Soc., 128, 371–394 (1838).

[62] L.M. Wilcox and R.S. Allison, Coarse-fine dichotomies in human stereopsis. Vision Res., 49, 2653-2665 (2009).